The Intraplate Stress Field of West Africa

Jean-Joel B. Legre[1], Yan Qin[2], Folarin Kolawole[3], and Tolulope Morayo Olugboji[1]

[1]University of Rochester
[2]Los Alamos National Laboratory
[3]Columbia University

December 14, 2023

Abstract

West Africa continues to host a growing number of low and intermediate-magnitude earth- quakes (M2-5) along its passive margins, and its continental interior. Earthquake activity in these regions raises the need to comprehend the causes and the tectonic controls of the seismicity. Unfortunately, such studies are rare. Here, we apply single-station inversion techniques to constrain fourteen focal mechanisms, computed after compiling a set of high- quality waveforms. We describe the connection between seismicity, the contemporary stress field, anthropogenic activity, and Holocene fault scarps in the region. Our results indicate transpressive stresses acting on the inherited brittle structures in the passive margins. We also observe a compressive regime in the intracontinental failed rifts. We attribute the seismicity to the reactivation of 'weak' faults in the Neoproterozoic and Mesozoic failed rifts, the passive transform structures, and the intracratonic Precambrian brittle shear zones.

Posted on 14 Dec 2023 — CC-BY 4.0 — https://doi.org/10.22541/au.170258905.55906211/v1 — This is a preprint and has not been peer-reviewed. Data may be preliminary.

The Intraplate Stress Field of West Africa

Jean-Joel Legre[1], Yan Qin[4], Folarin Kolawole[5], Tolulope Olugboji[1,2,3]

[1]Department of Earth and Environmental Sciences, University of Rochester, Rochester, NY, USA
[2]Department of Electrical and Computer Engineering, University of Rochester, Rochester, NY, USA
[3]Georgen Institute of Data Sciences, University of Rochester, Rochester, NY, USA
[4]Geophysics Group, Earth and Environmental Sciences Division, Los Alamos National Laboratory, NM
[5]Department of Earth and Environmental Sciences, Columbia University, New York City, NY, USA

Key Points:

- Improved constraints on stress regimes and stress orientations from inversion of new focal mechanisms of M $<$ 5.5 earthquakes.
- New focal mechanisms obtained from classical and a novel approach based on single station waveform inversion.
- Earthquakes in West Africa are rupturing the transform margin faults, intracontinental failed rift faults, and brittle shear zones.

Corresponding author: Jean-Joel Legre, `jlegre@ur.rochester.edu`

Abstract

West Africa continues to host a growing number of low and intermediate-magnitude earthquakes (M2-5) along its passive margins, and its continental interior. Earthquake activity in these regions raises the need to comprehend the causes and the tectonic controls of the seismicity. Unfortunately, such studies are rare. Here, we apply single-station inversion techniques to constrain fourteen focal mechanisms, computed after compiling a set of high-quality waveforms. We describe the connection between seismicity, the contemporary stress field, anthropogenic activity and Holocene fault scarps in the region. Our results indicate transpressive stresses acting on the inherited brittle structures in the passive margins. We also observe a compressive regime in the intracontinental failed rifts. We attribute the seismicity to the reactivation of 'weak' faults in the Neoproterozoic and Mesozoic failed rifts, the passive transform structures, and the intracratonic Precambrian brittle shear zones.

Plain Language Summary

Earthquakes have occurred in West Africa, in the interior and the edges of regions that host several brittle structures. The causes and the mechanisms of this seismicity have not been comprehensively investigated. Hence, the characteristics of the regional tectonics are not fully established. In this study, we resolve the properties of the source of earthquakes, and the regional stress field. Our description of the sources of earthquakes matches the geometry of inherited brittle shear zones and failed rifts. The results indicate a strong influence of transpressive stress transfer from the ocean to the passive margins of West Africa. In the continental interior, especially, the West African Belt, the stress is compressional in the E-W direction, consistent with stress orientations in adjoining regions. An extensional earthquake is observed in Mali, within the Gourma failed rift. We find that the seismicity of West Africa and the variations of the stress can be explained by the combination of preexisting faults, plate forces, ocean-continent stress transfer, and density heterogeneity across the geologic domains.

1 Introduction

West Africa is a region with a long history of tectonic deformation that spans Precambrian and Phanerozoic tectonics. Far away from the active tectonic boundaries at the Mid-ocean ridges and subduction zones, its continental interior hosts a plethora of earthquakes that are challenging to explain using simple tectonophysics models (Mbossi et al., 2021; Olugboji et al., 2021). These earthquakes are observed in clusters within and across the Neoproterozoic intra-cratonic failed rifts (i.e the Gourma Aulacogen), the Mesozoic failed rift systems, the passive transform margins, and the Precambrian brittle shear zones across the intra-cratonic shields (Figure 1b). The connections between the earthquake clusters and their causal factors are still unclear. One approach to understanding the driving mechanisms for these earthquakes is to study the stress patterns during faulting(Assumpção et al., 2016; Lithgow-Bertelloni & Guynn, 2004). However, the inferred stress field is sparse (Heidbach et al., 2018), primarily due to the limited seismological instrumentation across West Africa.

To date, much of what is known about Western Africa's stress field is inferred from the largest earthquakes along the transform passive margins (Kutu, 2013; Blundell, 1976; Langer et al., 1985; Nkodia et al., 2022a; Suleiman et al., 1993). As a result, the preferred mechanism invokes inherited structural weaknesses (i.e., local paleo-tectonics) and the transmission of far-field stresses from the ridges (i.e., regional contemporary-tectonics) (Nkodia et al., 2022a; Meghraoui et al., 2019). How applicable these explanations are for other earthquakes within the continental interiors, especially for smaller events, still remains uncertain. For example, the simple steady-state paradigm of regional stress-build up and release following strain accumulation is most likely unsuitable for earthquakes located far away from the passive margins (Calais et al., 2016; Sykes, 1978) where other mechanisms like gravitational effects could play a significant role (Coblentz & Sandiford, 1994; Heidbach et al., 2007; Sykes, 1978; Talwani, 2017). To investigate the controlling mechanisms on a larger set of West Africa's earthquakes , we provide new constraints on the orientation and the relative magnitude of the principal stresses across the continental interiors and along the passive margins. (Barth & Wenzel, 2010; Delvaux & Barth, 2010; Lund & Slunga, 1999).

Our appraisal of the stress field is based on a collection of new focal mechanisms calculated using fourteen moderate intraplate earthquakes. The crucial step involves estimating fault parameters using a single-station multimode body waveform inversion technique that is well suited to a sparse dataset (Brinkman et al., 2021; Jacob et al., 2022). Based on our new constraints, we explore all potential models that best explain the observed stress-field. These models are not limited to the ones identified above (i.e. structural weakness and tectonic forces), but are broad enough to explain a variable stress field across a variety of faulting modes. Therefore our discussion on causal models for explaining our results have been generalized so that they can: (1) explain the predominant orientation of earthquake stresses within the continental interior, (2) verify the observed stress regime along the passive margin and test the models that invoke stress transmission from the oceanic crust, (3) explore connections of earthquake nodal planes to exposed Holocene fault scarps within these passive transform margins, and (4) explain the disparity of slip modes across the *West Africa Craton.*

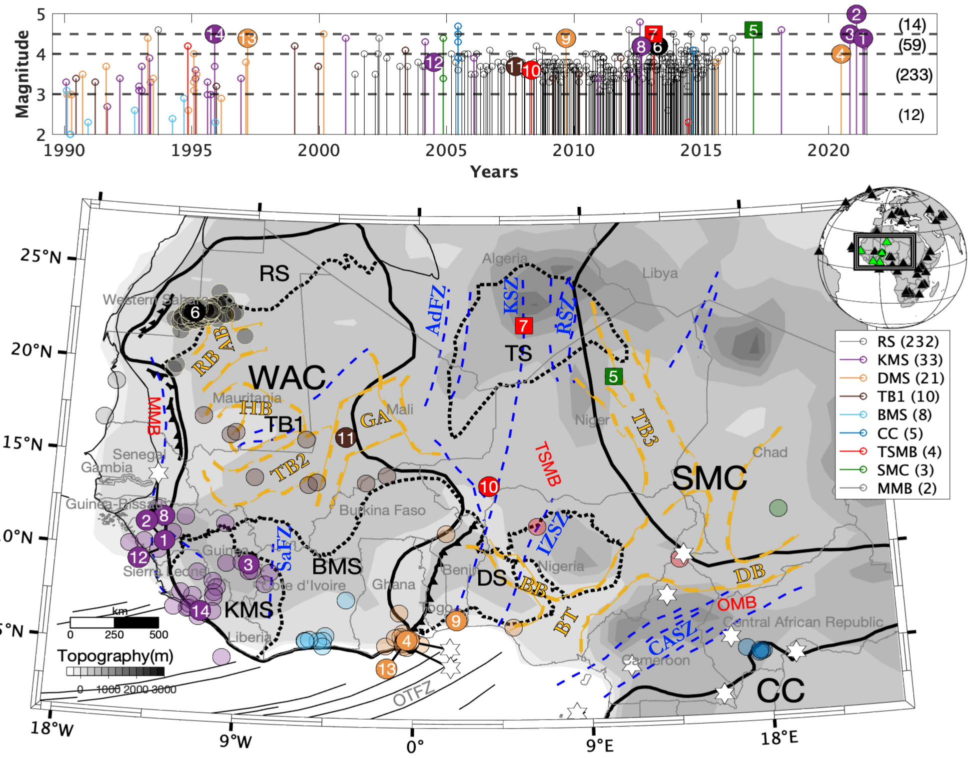

Figure 1. The spatio-temporal distribution of earthquakes located on continental West Africa and their relationship to basement domains. a) The time history of all events and a final list of fourteen events evaluated in this study (numbered symbols) . b) The epicenter of all events (similar to symbols in a). The focal mechanism solutions from other sources (white stars) are provided for reference. The major tectonic domains are: **I. Cratons** (thick black boundaries) : *WAC*, *SMC*, *CC*: *West Africa Craton*, *Sahara Metacraton*, *Congo Craton*; **II. Mobile Belts** (red text): *TSMB*, *OMB*, *MMB*: *Trans-Saharan Mobile Belt*, *Oubanguides Mobile Belt*, *Mauritanide Mobile Belt*; **III. Shields** (black dashed boundaries): *RS*, *KMS*, *BMS*, *DS*, *TS*: *Reguibat Shield*, *Kenema-Man Shield*, *Baoule-Mossi Shield*, *Dahomey Shield* and *Tuareg Shield*; **IV. Basins and Failed Rifts** (yellow dashed lines): *TB1*, *RB*, *AB*, *HB*, *TB2*, *GA*, *BB*, *BT*, *DB*, *TB3*: *Taoudeni Basin*; *Richat Basin*, *Adar Basin*, *Hodh Basin*, *Tambaoura Basin*, *Gourma Aulacogen*, *Bida Basin*, *Benue Trough*, *Doseo Basin*, *Termit Basin*; **V. Precambrian Ductile Shear Zones** (blue dashed lines): *KSZ*, *IZSZ*, *RSZ*, *CASZ*, *AdFZ*, *SaFZ* : *Kandi Shear Zone*, *Ifewara-Zungeru Shear Zone*, *Raghane Shear Zone*, *Central Africa Shear Zone*, *Adrar Fault*, *Sassandra Fault*; **VI. Oceanic Transform Fault Zones** (thin black lines): *OTFZ*. The inset shows the stations (black and green triangles) used in the determination of focal mechanisms (see Figures S1, S6). All geological domains introduced here are italicized in the rest of the manuscript.

2 Geologic Setting of Earthquakes in West Africa

The seismically active domains are located within regions that have either (1) experienced rifting episodes in the Neoproterozoic and Mesozoic (Albert-Villanueva et al., 2016; Begg et al., 2009), or (2) are located along brittle shear zones developed in the Archean and Neoproterozoic (Koffi et al., 2020). In the southwestern edge of the craton (*KMS*, Figure 1b), the faults are sinistral passive transform structures that are related to shear zones developed in the Mesoarchean and Eburnean, and they are oriented N-S, NNE-SSW, and WNW–ESE (Thiéblemont et al., 2004; Egal et al., 2002). Along the borders of the *Reguibat Shield*, the cluster of events is adjacent to fault zones developed in the Neoproterozoic Pan-African orogeny (750-550 Ma) (Black et al., 1994; Montero et al., 2016; Rocci et al., 1991), and the edges of a Neoproterozoic failed rift (underneath the *Richat* and *Adar Basins*, Figure 1b)(Affaton et al., 1991; Culver et al., 1991; Lécorché et al., 1991; Black et al., 1994; Grant, 1973). Several other rift segments and their brittle structures run through the platform beneath the *Taoudeni Basin*, the *Trans-Saharan Mobile Belt*, and the Western edge of the *Sahara Metacraton* (Figure 1b) (Albert-Villanueva et al., 2016; Begg et al., 2009; Caby et al., 1981). The *Trans-Saharan Mobile Belt* hosts earthquakes that are located along Precambrian shear zones, active during the Mesozoic strike-slip system in the region (Figure 1b)(Black et al., 1994; Caby & Bruguier, 2018; Fagbohun et al., 2020; J. Fairhead, 2023).

Much of the coastal seismicity in the Southern region (i.e., Ghana and Benin) reflects the control of transform structures (Figures 1b, 4f)(Burke, 1969; Kutu, 2013; Blundell, 1976). Geophysical studies have resolved some of the faults along the transform margin, and revealed the apparent connections to oceanic transform faults associated with the spreading of the Atlantic (J. D. Fairhead et al., 2013; Jessell et al., 2016). As we move further west from the coastal earthquakes in the Trans-Saharan Mobile belt, another cluster of coastal earthquakes are observed in Cote d'Ivoire (Mascle & Blarez, 1987; Blundell, 1976), within the southern *BMS*, and at its junction with the *DS* (Figure 1b). The faults trend NE-SW, similar to the transform faults that approach the coast of West Africa. Likewise, observations of transform structures on the western margin (i.e., Sierra Leone and Guinea) suggest a plausible connection to the Atlantic's fault system (Meghraoui et al., 2019). Although the relationship between onshore and offshore structures is not yet fully understood, the focal mechanisms of the two historical Ghanaian earthquakes are consistent with the current hypotheses. These events indicate a strike-slip regime (Suleiman et al., 1993; Yarwood & Doser, 1990) that are consistent with the kinematics along the oceanic transform faults (Yu et al., 2021). This study extends the focal mechanism catalog within this passive transform margin.

3 Data

We examined three decades (1991-2021) of seismic records (39,432 seismograms) retrieved from 62 stations using both global seismic networks (IRIS) and a regional seismic array-beam managed by the CTBTO (Comprehensive Nuclear Test Ban Treaty Organization). We identify high quality waveforms for low and intermediate-magnitude earthquakes (M2-5) with epicenters located on the West African continent. These earthquakes do not have focal mechanisms in the global CMT catalog . We determine waveform quality by inspecting the spectrograms and calculating the signal-to-noise ratio (SNR) of compressional and shear phases (PZ and ST). Earthquakes fall into three categories: highest quality (HQ), medium quality (MQ) and low quality (LQ) waveforms. Most of the events are not useful for our analysis because they are LQ. Therefore, we primarily focus on twelve events for single-station waveform inversion: four HQ and eight MQ events (Figure 2a). Only two earthquakes, in Algeria and Niger (labelled '5' and '7' in Figure 1), have enough waveforms to allow the estimation of focal mechanisms from the first compressional-motion technique. This is a total of 14 new focal mechanisms. A few example of our data selection process can be seen in Figure S3-S8.

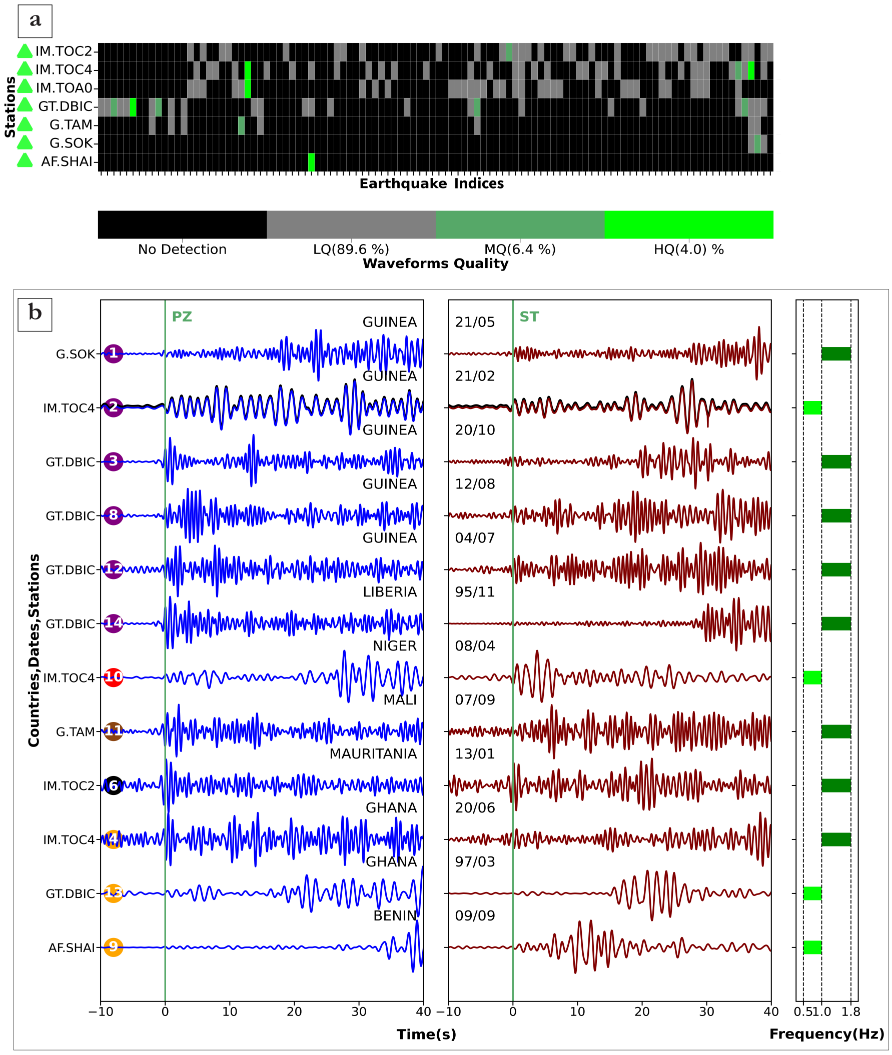

Figure 2. Classification of earthquake records based on waveform quality. a) A heat map showing the waveform quality assigned to all earthquakes recorded on seven of the quietest stations. Waveform quality is High Quality (HQ: bright green), Medium Quality (MQ: dark green, Low Quality (LQ: gray, only one phase, No detection (i.e. no pick or noisy earthquake waveforms). b) The best waveforms are plotted with reference to the PZ and ST picks at the optimal frequency bandwidth (the numbers beside the waveforms are similar to Figure 1).

4 Methods: Estimation of Focal Mechanisms & Stress Orientations

4.1 Single-Station Waveform Inversion for Focal Mechanisms

For twelve HQ events, we use a single-station body-wave fitting technique to solve for the optimal focal mechanism solutions. In the classical and modern extensions of this technique, the goal is to invert for the moment tensor by simulating synthetic waveforms and matching: (1) the compressional and shear body-wave phases (Dreger & Helmberger, 1993), (2) additional of surface reflected phases (Brinkman et al., 2021; Ferdinand & Arvidsson, 2002), or (3) surface wave phases (Maguire et al., 2023). Here, we focus on the body wave phases including later-arriving depth-phases (i.e., sP, PP , sS, and SS) (Brinkman et al., 2021). A grid search for the plausible orientations of double-couple solutions (i.e, strike, dip, rake), and the earthquake depth, is conducted using the filtered waveforms. The optimal solution retains lowest misfits (Figure 3a). In computing the synthetic seismograms, we filter using same frequencies as the observed data, and windowed the waveforms between -1 second and 12 seconds (Figure 3b). We supplement our fourteen new focal mechanism solutions (Table S2) with three obtained from previous studies (Table S1).

4.2 Focal Mechanisms Inversion for Stress Orientations & Regimes

We apply a stress inversion technique that is a hybrid of the iterative linear scheme of (Vavryčuk, 2014) and the damped least squares approach of (Martinez-Garzon et al., 2014; Hardebeck & Michael, 2006). The final solution obtained is a set of four parameters: a single stress magnitude, R, and the orientations (plunge and trend) for the principal stresses (i.e., $\sigma_1 \geq \sigma_2 \geq \sigma_3$). This solution, chosen to fit the dataset of fault parameters (i.e., strikes, dips, and rakes), is obtained by minimizing the fit between the slip vector and the shear traction on each fault plane (Angelier, 1984). Initial solutions are calculated without any knowledge of the fault plane. These values are then used to evaluate each of the nodal planes to determine the most unstable plane (Lund & Slunga, 1999; Lund, 2000; Vavryčuk, 2014). The true fault plane is the nodal plane with the highest value of Coloumb failure stress. Subsequent iterations then refine the initial stress field using the correctly identified fault plane solutions (Vavryčuk, 2014; Lavayssière et al., 2019). The 'stress regime' is determined by identifying which of the principal stresses axes are vertical (or near vertical) and evaluating a stress-regime index that enables classification into non-Andersonian fault types (Delvaux et al., 1997; Nkodia et al., 2022b; Sperner, 2003). Finally, we estimate the direction of maximum horizontal stress following the technique of (Lund & Townend, 2007; Martinez-Garzon et al., 2014).

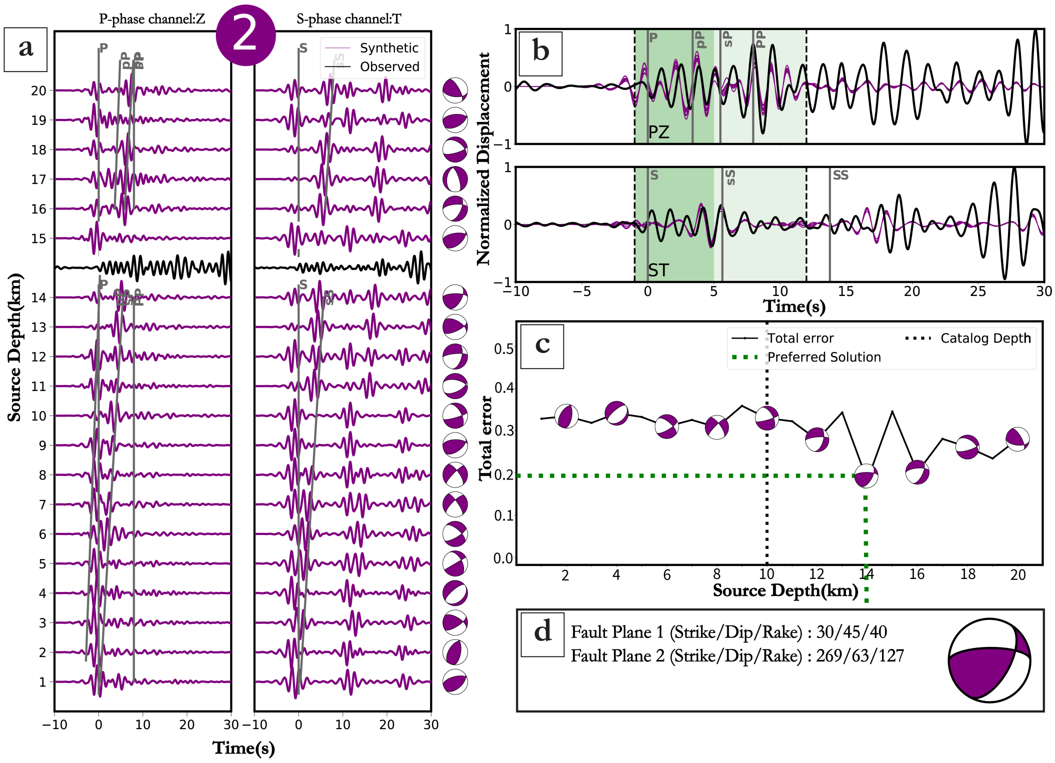

Figure 3. A description of the single station moment tensor inversion. a) Normalized waveforms of PZ and ST phases filtered. The focal mechanisms indicate the preferred fault geometry at different depths. b) The recorded waveform is iteratively fitted to each synthetic waveform. A weighted parameterization is prescribed on the time window (-1 s to 12 s) used in the inversion: 10 (dark green window width, 6 s), and 1 (light green window width, 7 s). c) Models of earthquake sources with respect to phase misfits between the observed and synthetic waveforms. The lowest misfit source solution for earthquake '2' is identified at a depth of 14 km. d) The fault plane and auxiliary plane for the best-fit focal mechanism in c).

5 Results: Mechanisms of the Seismicity in West Africa

5.1 Heterogeneous Faulting Mode & Horizontal Stress Field

The *KMS* is the best-constrained in this study. We resolve six new focal mechanisms. The result suggests strike-slip and compressional tectonics. Two events show normal faulting (see Figure 1, Figures 4a,b, and Table S1). The maximum orientation of the transpressive regional stress regime is almost perpendicular to the edge of the western passive margin (Figure 4d). The next best resolved region is on the southeastern margin of West Africa, near the *DS* (see Table S1). The new solutions indicate reverse and normal faulting. The maximum horizontal stress for these events trend SW-NE (Figure 4a, 4e, Table S2). On the coast of Benin, we resolved a, SSE-NNW compressional event (Figure 4a and 4e), which is consistent with previous estimates (white circles in Figure 4e). In the southern-eastern passive margin, the regional stress inversion suggests a N-S transpressive stress regime (Figure 4f). Within the cluster of Mauritania events we resolve only a single focal mechanism solution (strike-slip event with a compressive component and a N-S oriented shmax). Along the *GA*, we resolved a normal faulting mechanism with a nodal plane oriented in a NE-SW direction (Figure 4a, 4e). Finally, near the edge of the *Trans-Saharan Mobile Belt*, our results suggests a widespread reverse style of fault motions. In this region, the orientations of the nodal planes are consistent with published descriptions of fault networks in the Tuareg region (i.e, Algeria, Niger in Figure 4a). This is because most of the lineaments imaged from magnetic and gravity data show patterns that are approximately oriented either N-S, NE-SW or SE-NW (Brahimi et al., 2018). In general, the orientation of the maximum horizontal stresses varies from the south to the north. Below the *TB3*, (Figure 4e), the stress is oriented NW-SE.

5.2 Earthquake Depth: Faulting in the Brittle Regime

The depths of our focal mechanisms are clustered in the shallow crust (<20 km - see Figure 4b). We note significant depth variations across West Africa from one basement domain to another (Figure 4b). The earthquake hypocenters in the *KMS* occupy a larger depth range. The most recent events in that area occurred deeper (10-20) km in the crust than the earliest event (compare '1-3', to '8','12','14', Figures 1 and 4). In the *RS*, the single resolved event from the Mauritania cluster is located at a depth of 20 km in the crust. We obtain a similar depth solution for the focal mechanism in the *TB-1*. The sources of the earthquakes in the southeastern passive margin (i.e., '4', '9', and '13', Figures 1 and 4) indicate a seismogenic zone in the range 15-20 km, while shallower seismicity (5-10 km) is observed in the *TSMB*.

6 Discussion: Tectonic Implications

The basement of West Africa is riddled with numerous faults that constitute regions of mechanical weaknesses that may explain the seismogenesis in the region. The co-location of earthquakes and previously mapped brittle discontinuities in West Africa argues for the influence of preexisting structures on the seismicity along the coast (e.g., Burke, 1969; Olugboji et al., 2021; Nkodia et al., 2022). For the newly resolved focal mechanisms within the interior of the continent, we argue that the seismicity may also be related to the weak state of brittle fault zones that were developed during the Precambrian orogenies as well as Precambrian and Mesozoic rifting episodes. This suggests the relative instability of the craton (Sykes, 1978; Thomas & Powell, 2017), and is confirmed by the heterogeneity of the resolved stress regimes (Figure 4e-f). We also note the absence of earthquakes in provinces with few-to-no published brittle deformation structures (e.g., the eastern *RS*, and the *BMS*) (Figure 1b). The distinct stress regimes and orientations of the earthquakes (Figure 4e) translate disparate influences across the region and require a subdivision into two categories (i.e., Passive Transform Margins, and Continental interiors).

6.1 Inherited Passive Transform Margin Structures

Previous attempts to understand the seismicity of West African margins have suggested that the principal driver of fault reactivation is the transfer of offshore stress (Nkodia et al., 2022a; Suleiman et al., 1993). To first order, our results confirm this interpretation. The resolved horizontal stresses show a close alignment with the kinematics of the oceanic transform faults (Burke, 1969). Along the Ghanian-Togo Passive Transform Margin, Burke (1969) reported the presence of 40-km long fault scarps (Lokossa Fault, LF and Sehoue Fault, SF in Figure 4f, 4g). We identify another fault scarp in the vicinity of the previously reported ones (dubbed 'Apessito' Fault, APF, Figure 4g). The scarp is colinear to the nearest passive transform margin (Figures 4g). This further supports the hypothesis that the paleo-transform faults are accommodating surface-rupturing and reactivation. Furthermore, exhumed Precambrian basement terranes near the southern edge of the Dahomey Shield (SW Nigeria; 'DS' in Figure 1b) record pervasive ENE-to-NE trending mega-fractures, parallel to the trend of the offshore fracture zones (Odeyemi et al., 1999; Anifowose & Kolawole, 2012).

The connection between offshore transform margin faults, recent onshore fault scarps, and the mechanism of seismic reactivation on the margins is not sufficient to explain the stress in the Guinea-Liberia margins of the *KMS*. The pattern and orientation of the ambient stress, inferred require a more different mechanism. Few of the stresses show local extensions in the crust (Figure 4a,e). This is congruent with the tectonic evolution of the region. The margin-proximal earthquakes retain a memory of Mesozoic extension associated with the opening of the Atlantic Ocean. Moreover, near the coast of Liberia, the orientation of the horizontal stress, evokes the role of local features (e.g., sediment load inducing flexural stresses). This is similar to the interpretation of stress characteristics on the northeast margin of South America (i.e., Brazil's coast) which experienced a similar tectonic history (Assumpção et al., 2016).

6.2 Induced Seismicity

We associate the largest seismic cluster in the Western *Reguibat Shield* to anthropogenic re-activation of brittle discontinuities that are collocated with the Kedia D'Idjill iron ore mines in Mauritania (Figure 4c). The similarity between a preferred nodal plane and the orientation of exposed transcurrent faults suggests a contributing influence of the transpressive collisional tectonics along the northern margin of Africa (Meghraoui & Pondrelli, 2012). The spatio-temporal sequence of the earthquakes (Figures 4b, S2) indicates that mining activity introduced Coulomb stress transfer, causing a large spike in seismicity between 2001 and 2017, (e.g., (Qin et al., 2018)). Unfortunately, further analysis is not possible at this time, because of the poor quality of seismic data for these events.

6.3 Reactivation of Failed Rifts in Continental Interior

The three main regions with failed rifts are: The *Trans-Saharan Mobile Belt*(*TSMB*), the Sahara metacraton (*SMC*), and the *Gourma Aulacogen* (*GA*). These structures are mainly reactivated in compressional style, with the exception of the *GA* (which hosted an extensional event), suggesting vertical perturbation in the local stress. Nevertheless, the orientation of maximum horizontal stress stays consistent across the northern part of the *TSMB*, the *GA*, and part of the *Oubanguides Mobile Belt*. The only instance of rotation is noted at the edge of the *SMC*. This could arise from the effect of lateral density contrast (Humphreys & Coblentz, 2007) between the *TSMB* and the *SMC* (Zoback et al., 2009).

6.4 Current Limitations and Future Work

The stress field we have presented here, although compelling and useful for addressing the influence of tectonic and non-tectonic forces on the pattern of observed seismicity, still retains non-negligible uncertainties. The uncertainities result primarily from a sparsity of focal mechanism solutions which propagate into uncertainties in the inferred stress orientations. We are aware that the use of single-station observations may result in large uncertainties in the inferred earthquake moment tensor solutions. That said, our results provide the best compilation of intermediate magnitude focal mechanism solution extending inland away from the passive margins. This caveat noted, we argue for our preferred solution based on the good correspondence with the observed faults in the regions (Caby & Bruguier, 2018; Fagbohun et al., 2020). Also, the self-consistency within the different clusters of seismicity reinforces the plausibility of our preferred solutions. Future work should address observational gaps. The targets include improved instrumentation around the identified earthquake clusters or algorithmic approaches such as template matching.

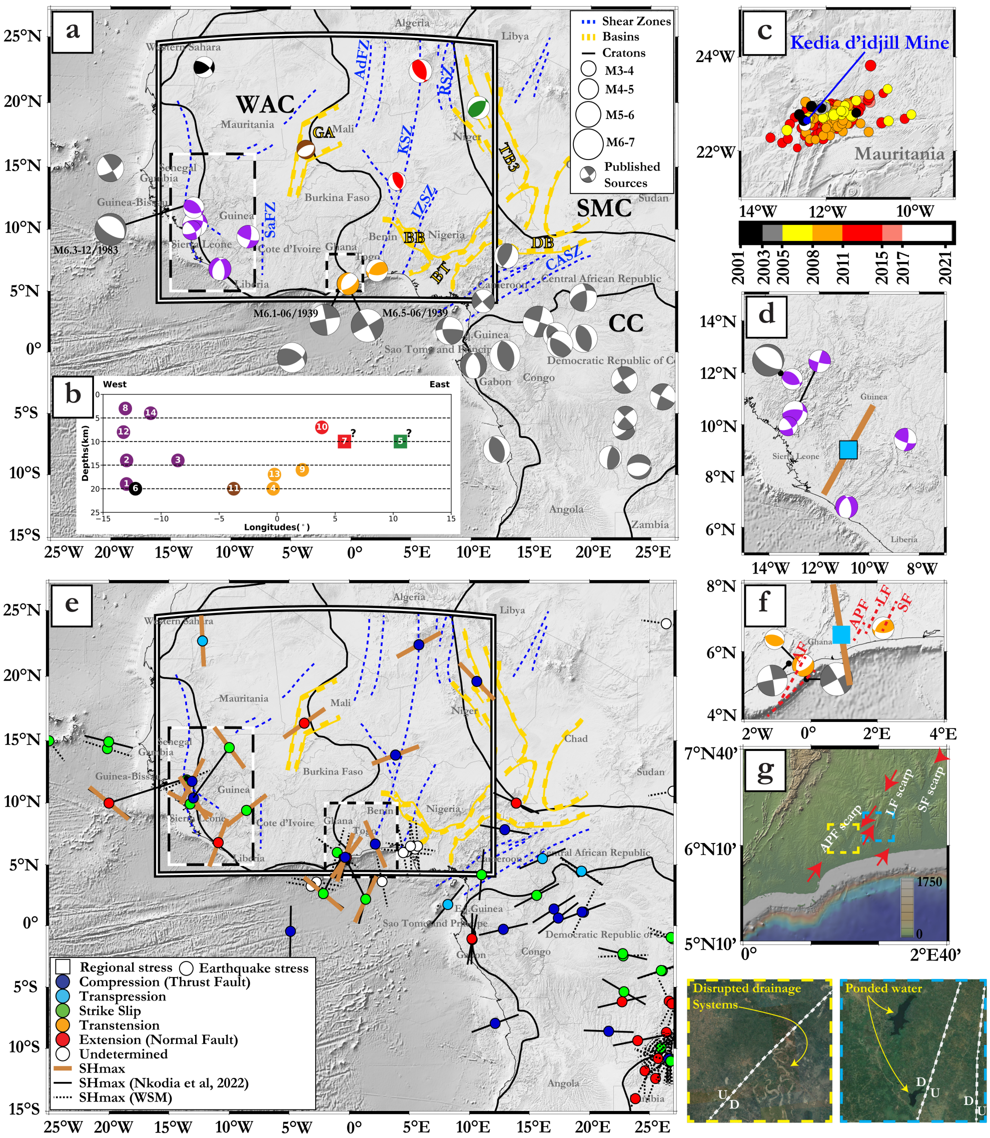

Figure 4. The focal mechanisms and stress field for West and Central Africa. a) Results from this study (in colors and identified by squared region). b) Earthquake depth with question marks identifying unresolved depths. c) The spatio-temporal sequence in the Reguibat cluster relative to the location of the Kedia D'idjill Mine. d) The regime and orientation of maximum horizontal stress for the Western passive margin. e) The stress regime and orientation of maximum horizontal stress for the individual earthquakes in Western and Central Africa (supplemented by other studies). f) The result of the regional inversion showing stress regime and orientation of maximum horizontal stress for the southeastern passive margin. The Holocene faults (red dashed lines): AF, LF, SF, APF: Akwapim Fault, Lokossa Fault, Sehoue Fault, Apessito Fault. g) The scarps of the faults in the southeastern transform passive margin. The disruption of water channels are observed in the dashed yellow and blue squared areas, corresponding to the Apessito fault scarp and the Lokossa fault scarp. The motion along the faults is described as U (upward) and D (downward). The solutions in 4a and 4b are color-coded and numbered similar to Figure 1b

.

7 Conclusion

We investigated three decades of seismicity and provide new constraints on the stress field in West Africa. The results suggest that the stress field: (1) is in the transpressive regime and controlled by a stress transfer from the oceanic crust to the passive transform margins of West Africa, (2) is influenced by the presence of fault scarps in the southern passive transform margins, (3) is in different regimes for earthquakes located within the *West Africa Craton* compared to those along the *Trans-Saharan Mobile Belt*, (4) may be driven by anthropogenic perturbations within the *Reguibat Shield*, and (5) is influenced by transpressive stresses transmitted from northern Africa tectonics into the continental interior. A better view of the stress field will require significant improvements in the station coverage, especially along the rim of West African terranes where most of the earthquakes occur.

8 Supplementary Information

Our compilation of data is complemented by eighteen compressional waveforms that captured the vibration field of the M4.5, valentine 2013 earthquake, and the M4.6 - 01/18/2017, southern-Algeria earthquake (Figure S10). We report the parameters of our focal mechanisms, and the historical seismicity in Table S2 and S3.

9 Acknowledgements

We appreciate the Comprehensive Nuclear-Test-Ban Treaty (CTBTO) for granting access to the seismic records from the beam IM.TORD, located in Torodi, Niger. The dataset was pivotal in the furtherance and the outcome of this investigation. We thank Nienke Brinkman and Simon Stähler for the communication of information concerning the implementation of the Single-Station Moment Tensor Inversion. We also thank Lara Wagner, Baowei Liu, and the members of the seismological laboratory at the University of Rochester (URSeismo) for insightful discussions. Finally, we acknowledge the financial support from the National Science Foundation under grant number: 2102495. Data used in this study can be obtained from the IRIS data management center (http://ds.iris.edu/ds/).

10 Open Research

The dataset used in this study can be retrieved from IRIS using Obspy's routines for mass download. The software for this task is accessible in the Github repository linked to the DOI: 10.5281/zenodo.10368838. The repository contains the specific information for the earthquakes and the stations — all seismic data from the IM.TORD beam is private and can only be requested from the CTBTO. The waveforms in this study are trimmed to focus on the compressional and shear phases, after calculations of travel time using the Obspy library version 1.2.2, the IASP91 velocity model, and the time corrections reported in the tables for the earthquakes and stations.

References

Affaton, P., Rahaman, M. A., Trompette, R., & Sougy, J. (1991). The dahomeyide orogen: Tectonothermal evolution and relationships with the volta basin. In R. D. Dallmeyer & J. P. Lécorché (Eds.), *The west african orogens and Circum-Atlantic correlatives* (pp. 107–122). Berlin, Heidelberg: Springer Berlin Heidelberg.

Albert-Villanueva, E., Permanyer, A., Tritlla, J., Levresse, G., & Salas, R. (2016). Solid hydrocarbons in proterozoic dolomites, taoudeni basin, mauritania. *Journal of Petroleum Geology*, *39*(1), 5-27.

Angelier, J. (1984). Tectonic analysis of fault slip data sets. *J. Geophys. Res. [Solid Earth]*.

Anifowose, A., & Kolawole, F. (2012). Emplacement tectonics of idanre batholith, west africa. *Comunicação Geológicas*, *99*(2).

Assumpção, M., Dias, F. L., Zevallos, I., & Naliboff, J. B. (2016). Intraplate stress field in south america from earthquake focal mechanisms. *Journal of South American Earth Sciences*, *71*, 278–295.

Barth, A., & Wenzel, F. (2010, February). New constraints on the intraplate stress field of the amurian plate deduced from light earthquake focal mechanisms. *Tectonophysics*, *482*(1-4), 160–169.

Begg, G. C., Griffin, W. L., Natapov, L. M., O'Reilly, S. Y., Grand, S. P., O'Neill, C. J., ... Bowden, P. (2009, February). The lithospheric architecture of africa: Seismic tomography, mantle petrology, and tectonic evolutionthe lithospheric architecture of africa. *Geosphere*, *5*(1), 23–50.

Black, R., Latouche, L., Liegeois, J. P., Caby, R., & Bertrand, J. M. (1994, July). Pan-African displaced terranes in the tuareg shield (central sahara). *Geology*, *22*(7), 641–644.

Blundell, D. (1976). Active faults in west africa. *Earth and Planetary Science Letters*, *31*(2), 287–290.

Brahimi, S., Liégeois, J.-P., Ghienne, J.-F., Munschy, M., & Bourmatte, A. (2018, October). The tuareg shield terranes revisited and extended towards the northern gondwana margin: Magnetic and gravimetric constraints. *Earth-Sci. Rev.*, *185*, 572–599.

Brinkman, N., Stähler, S. C., Giardini, D., Schmelzbach, C., Khan, A., Jacob, A., ... others (2021). First focal mechanisms of marsquakes. *Journal of Geophysical Research: Planets*, *126*(4), e2020JE006546.

Burke, K. (1969). Seismic areas of the guinea coast where atlantic fracture zones reach africa. *Nature*, *222*(5194), 655–657.

Caby, R., Bertrand, J. M. L., & Black, R. (1981, January). Chapter 16 Pan-African ocean closure and continental collision in the Hoggar-Iforas segment, central sahara. In A. Kröner (Ed.), *Developments in precambrian geology* (Vol. 4, pp. 407–434). Elsevier.

Caby, R., & Bruguier, O. (2018). A subducted neoproterozoic rift assemblage: the egere group (central hoggar, algeria). *Journal of African Earth Sciences*, *147*, 544–553.

Calais, E., Camelbeeck, T., Stein, S., Liu, M., & Craig, T. J. (2016, October). A new paradigm for large earthquakes in stable continental plate interiors: LARGE EARTHQUAKES IN SCRs. *Geophys. Res. Lett.*, *43*(20), 10,621–10,637.

Coblentz, D. D., & Sandiford, M. (1994, September). Tectonic stresses in the african plate: Constraints on the ambient lithospheric stress state. *Geology*, *22*(9), 831–834.

Culver, S., Williams, H., & Venkatakrishnan, R. (1991). The rokelide orogen. In *The west african orogens and circum-atlantic correlatives* (pp. 123–150). Springer.

Delvaux, D., & Barth, A. (2010, February). African stress pattern from formal inversion of focal mechanism data. *Tectonophysics*, *482*(1), 105–128.

Delvaux, D., Moeys, R., Stapel, G., Petit, C., Levi, K., Miroshnichenko, A., ... San'kov, V. (1997). Paleostress reconstructions and geodynamics of the baikal region, central asia, part 2. cenozoic rifting. *Tectonophysics*, *282*(1-4), 1–38.

Dreger, D. S., & Helmberger, D. V. (1993, May). Determination of source parameters at regional distances with three-component sparse network data. *J. Geophys. Res.*, *98*(B5), 8107–8125.

Egal, E., Thiéblemont, D., Lahondère, D., Guerrot, C., Costea, C. A., Iliescu, D., ... Kolié, P. (2002, July). Late eburnean granitization and tectonics along the western and northwestern margin of the archean Kénéma–Man domain (guinea, west african craton). *Precambrian Res.*, *117*(1), 57–84.

Fagbohun, B. J., Omitogun, A. A., Bamisaiye, O. A., & Ayoola, F. J. (2020, January). Gold potential of the pan african Trans-Sahara belt and prospect for further exploration. *Ore Geol. Rev.*, *116*, 103260.

Fairhead, J. (2023). The mesozoic west and central africa rift system (wcars) and the older kandi shear zone (ksz): Rifting and tectonics of north africa and south america and fragmentation of gondwana based on geophysical investigations. *Journal of African*

Earth Sciences, *199*, 104817.
Fairhead, J. D., Green, C. M., Masterton, S. M., & Guiraud, R. (2013, May). The role that plate tectonics, inferred stress changes and stratigraphic unconformities have on the evolution of the west and central african rift system and the atlantic continental margins. *Tectonophysics*, *594*, 118–127.
Ferdinand, R. W., & Arvidsson, R. (2002, October). The determination of source mechanisms of small earthquakes and revised models of local crustal structure by moment tensor inversion. *Geophys. J. Int.*, *151*(1), 221–234.
Grant, N. K. (1973). Orogeny and reactivation to the west and southeast of the west african craton. In A. E. M. Nairn & F. G. Stehli (Eds.), *The south atlantic* (pp. 447–492). Boston, MA: Springer US.
Hardebeck, J. L., & Michael, A. J. (2006). Damped regional-scale stress inversions: Methodology and examples for southern california and the coalinga aftershock sequence. *Journal of Geophysical Research: Solid Earth*, *111*(B11).
Heidbach, O., Rajabi, M., Cui, X., Fuchs, K., Müller, B., Reinecker, J., … Zoback, M. (2018, October). The world stress map database release 2016: Crustal stress pattern across scales. *Tectonophysics*, *744*, 484–498.
Heidbach, O., Reinecker, J., Tingay, M., Müller, B., & others. (2007). Plate boundary forces are not enough: Second-and third-order stress patterns highlighted in the world stress map database.
Humphreys, E. D., & Coblentz, D. D. (2007). North american dynamics and western US tectonics. *Rev. Geophys.*.
Jacob, A., Plasman, M., Perrin, C., Fuji, N., Lognonné, P., Xu, Z., … Banerdt, W. B. (2022, August). Seismic sources of InSight marsquakes and seismotectonic context of elysium planitia, mars. *Tectonophysics*, *837*, 229434.
Jessell, M. W., Begg, G. C., & Miller, M. S. (2016, March). The geophysical signatures of the west african craton. *Precambrian Res.*, *274*, 3–24.
Koffi, G. R.-S., Kouamelan, A. N., Allialy, M. E., Coulibaly, Y., & Peucat, J.-J. (2020, March). Re-evaluation of leonian and liberian events in the geodynamical evolution of the Man-Leo shield (west african craton). *Precambrian Res.*, *338*, 105582.
Kutu, J. M. (2013). Seismic and tectonic correspondence of major earthquake regions in southern ghana with mid-atlantic transform-fracture zones. *International Journal of Geosciences*, *2013*.
Langer, C. J., Bonilla, M. G., & Bollinger, G. A. (1985). *The guinea, west africa, earthquake of december 22, 1983; reconnaissance geologic and seismologic field studies* (Tech. Rep.). US Geological Survey,.
Lavayssière, A., Drooff, C., Ebinger, C., Gallacher, R., Illsley-Kemp, F., Oliva, S. J., & Keir, D. (2019). Depth extent and kinematics of faulting in the southern tanganyika rift, africa. *Tectonics*, *38*(3), 842–862.
Lécorché, J. P., Bronner, G., Dallmeyer, R. D., Rocci, G., & Roussel, J. (1991). The mauritanide orogen and its northern extensions (western sahara and zemmour), west africa. In R. D. Dallmeyer & J. P. Lécorché (Eds.), *The west african orogens and Circum-Atlantic correlatives* (pp. 187–227). Berlin, Heidelberg: Springer Berlin Heidelberg.
Lithgow-Bertelloni, C., & Guynn, J. H. (2004). Origin of the lithospheric stress field. *Journal of Geophysical Research: Solid Earth*, *109*(B1).
Lund, B. (2000). *Crustal stress studies using microearthquakes and boreholes* (Unpublished doctoral dissertation).
Lund, B., & Slunga, R. (1999, July). Stress tensor inversion using detailed microearthquake information and stability constraints: Application to ölfus in southwest iceland. *J. Geophys. Res.*, *104*(B7), 14947–14964.
Lund, B., & Townend, J. (2007, September). Calculating horizontal stress orientations with full or partial knowledge of the tectonic stress tensor. *Geophys. J. Int.*, *170*(3), 1328–1335.
Maguire, R., Lekić, V., Kim, D., Schmerr, N., Li, J., Beghein, C., … Banerdt, W. B. (2023, September). Focal mechanism determination of event s1222a and implications

for tectonics near the dichotomy boundary in southern elysium planitia, mars. *J. Geophys. Res. Planets*, *128*(9).

Martinez-Garzon, P., Kwiatek, G., Ickrath, M., & Bohnhoff, M. (2014). *MSATSI: A MATLAB package for stress inversion combining solid classic methodology, a new simplified User-Handling, and a visualization tool* (Vol. 85) (No. 4).

Mascle, J., & Blarez, E. (1987). Evidence for transform margin evolution from the ivory coast–ghana continental margin. *Nature*, *326*(6111), 378–381.

Mbossi, E. F., Ndibi, D. D. E., Nguet, P. W., Abate Essi, J. M., Biboum Ntomb, E. O., Dili-Rake, J., ... Tabod, T. C. (2021, April). Preliminary seismic hazard assessment in west africa based on incomplete seismic catalogs. *Open J. Earthq. Res.*, *10*(02), 75–93.

Meghraoui, M., Amponsah, P., Bernard, P., & Ateba, B. (2019). Active transform faults in the gulf of guinea: insights from geophysical data and implications for seismic hazard assessment. *Canadian Journal of Earth Sciences*, *56*(12), 1398–1408.

Meghraoui, M., & Pondrelli, S. (2012). Active faulting and transpression tectonics along the plate boundary in north africa. *Annals of Geophysics*, *55*(5), pp–955.

Montero, P., Haissen, F., Mouttaqi, A., Molina, J. F., Errami, A., Sadki, O., ... Bea, F. (2016). Contrasting SHRIMP U–Pb zircon ages of two carbonatite complexes from the peri-cratonic terranes of the reguibat shield: Implications for the lateral extension of the west african craton. *Gondwana Res.*, *38*, 238–250.

Nkodia, H. M. D.-V., Miyouna, T., Kolawole, F., Boudzoumou, F., Loemba, A. P. R., Bazebizonza Tchiguina, N. C., & Delvaux, D. (2022a). Seismogenic fault reactivation in western central africa: Insights from regional stress analysis. *Geochem. Geophys. Geosyst.*, *23*(11), e2022GC010377.

Nkodia, H. M. D.-V., Miyouna, T., Kolawole, F., Boudzoumou, F., Loemba, A. P. R., Bazebizonza Tchiguina, N. C., & Delvaux, D. (2022b). Seismogenic fault reactivation in western central africa: Insights from regional stress analysis. *Geochemistry, Geophysics, Geosystems*, *23*(11), e2022GC010377.

Odeyemi, I., Asiwaju-Bello, Y., & Anifowose, A. (1999). Remote sensing fracture characteristics of pan african granite batholiths in the basement complex of parts of south western nigeria. *The Journal of Technoscience*, *3*, 56–60.

Olugboji, T., Shirzaei, M., Lu, Y., Adepelumi, A. A., & Kolawole, F. (2021). On the origin of orphan tremors and intraplate seismicity in western africa. *Frontiers in Earth Science*, *9*, 716630.

Qin, Y., Chen, X., Carpenter, B. M., & Kolawole, F. (2018, October). Coulomb stress transfer influences fault reactivation in areas of wastewater injection. *Geophys. Res. Lett.*, *45*(20), 11,059–11,067.

Rocci, G., Bronner, G., & Deschamps, M. (1991). Crystalline basement of the west african craton. In R. D. Dallmeyer & J. P. Lécorché (Eds.), *The west african orogens and Circum-Atlantic correlatives* (pp. 31–61). Berlin, Heidelberg: Springer Berlin Heidelberg.

Sperner, B. (2003). New aspects of tectonic stress inversion with reference to the tensor program. *Geological Society, London, Special Publications*, *212*(1), 75–100.

Suleiman, A. S., Doser, D. I., & Yarwood, D. R. (1993, June). Source parameters of earthquakes along the coastal margin of west africa and comparisons with earthquakes in other coastal margin settings. *Tectonophysics*, *222*(1), 79–91.

Sykes, L. R. (1978). Intraplate seismicity, reactivation of preexisting zones of weakness, alkaline magmatism, and other tectonism postdating continental fragmentation. *Reviews of Geophysics*, *16*(4), 621–688.

Talwani, P. (2017, January). On the nature of intraplate earthquakes. *J. Seismol.*, *21*(1), 47–68.

Thiéblemont, D., Goujou, J. C., Egal, E., Cocherie, A., Delor, C., Lafon, J. M., & Fanning, C. M. (2004, June). Archean evolution of the leo rise and its eburnean reworking. *J. Afr. Earth. Sci.*, *39*(3), 97–104.

Thomas, W. A., & Powell, C. A. (2017). Necessary conditions for intraplate seismic zones

in north america. *Tectonics*, *36*(12), 2903–2917.
Vavryčuk, V. (2014, July). Iterative joint inversion for stress and fault orientations from focal mechanisms. *Geophys. J. Int.*, *199*(1), 69–77.
Yarwood, D. R., & Doser, D. I. (1990, February). Deflection of oceanic transform motion at a continental margin as deduced from waveform inversion of the 1939 accra, ghana earthquake. *Tectonophysics*, *172*(3), 341–349.
Yu, Z., Singh, S. C., Gregory, E. P. M., Maia, M., Wang, Z., & Brunelli, D. (2021). *Semibrittle seismic deformation in high-temperature mantle mylonite shear zone along the romanche transform fault* (Vol. 7) (No. 15).
Zoback, M. L., Zoback, M. D., Watts, A., & Schubert, G. (2009). Lithosphere stress and deformation. *Crust and lithosphere dynamics: Elsevier*, 253–273.

Supplementary Materials for:

The Intraplate Stress Field of West Africa

Jean-Joel Legre[1], Yan Qin[4], Folarin Kolawole[5], Tolulope Olugboji[1,2,3]

[1]Department of Earth and Environmental Sciences, University of Rochester, Rochester, NY, USA
[2]Department of Electrical and Computer Engineering, University of Rochester, Rochester, NY, USA
[3]Georgen Institute of Data Sciences, University of Rochester, Rochester, NY, USA
[4]Geophysics Group, Earth and Environmental Sciences Division, Los Alamos National Laboratory, NM
[5]Department of Earth and Environmental Sciences, Columbia University, New York City, NY, USA

This file contains: Figure S1-11 and Table S1-2

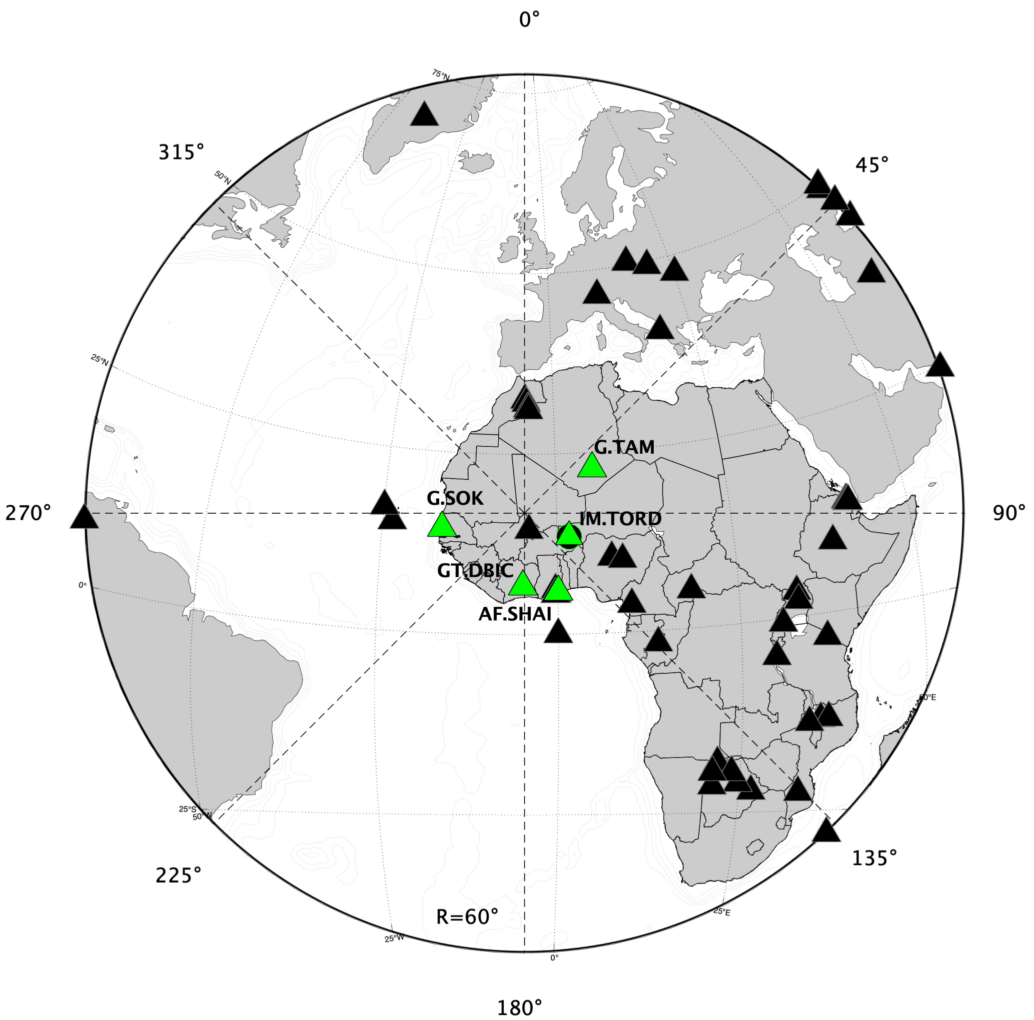

Figure S 1. Locations of the 62 stations (i.e. 58 stations from IRIS (triangles), and four(4) stations from the IM.TORD array (black circle overlaid by green triangle)) used in the selection of seismic data from West Africa's earthquakes. The green triangles show the stations that were used in the single station inversions for moment tensors after the automatic pick of PZ and ST phases, and their accurate identification through observational arrival time corrections.

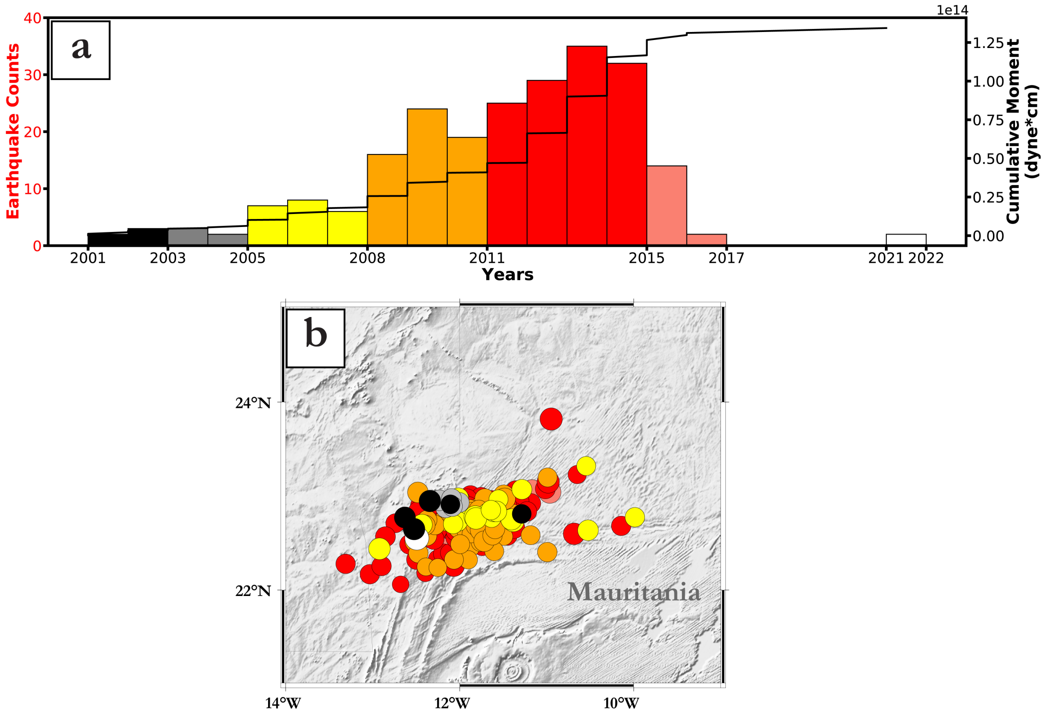

Figure S 2. Sequence of activation of the seismogenic structures related to the Reguibat cluster of earthquakes. a) Histogram of earthquakes and cumulative sum of their seismic moment (black line) showing five (5) phases of activities, which are marked by the rise in the number and the cumulative size of events. b) Spatial evolution of the sequence of earthquakes based on the range of years indicated in the plot (a).

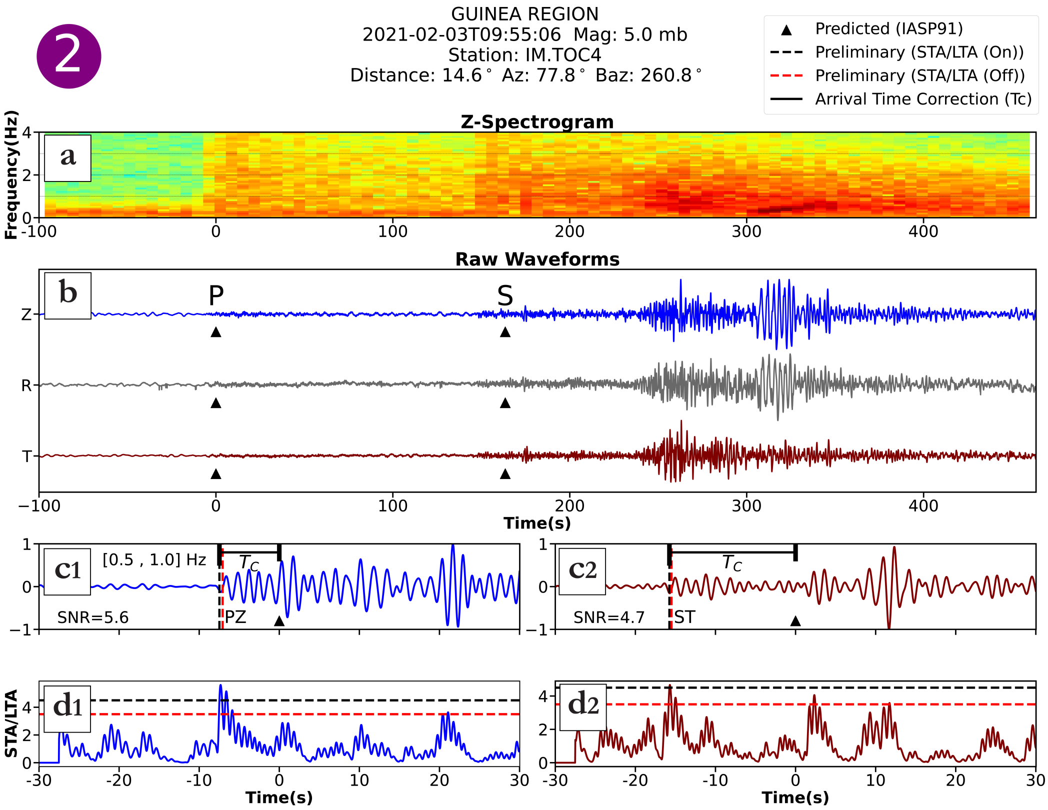

Figure S 3. An example of the procedure of automatic phase detection and SNR estimation used for identification of a high-quality (HQ) waveform. a) The spectrogram of ground vibrations recorded on the vertical channel, plotted with reference to the first arrival time of the compressional wave. b) The unfiltered waveforms recorded on the vertical (Z), Radial (R), and the Transverse (T) channels with predicted arrival times for P and S body-wave phases (black triangles). c1-c2) The bandpass filtered (0.5-1.0Hz: optimal for HQ) waveforms showing the estimated arrival times (dashed lines) of compressional wave on the vertical channel (PZ) and the shear wave on the transverse channel (ST). The actual arrival time differs slightly from the theoretical arrival time (compare triangle to dashed lines). The compressional and shear wave arrived -7.3 s and -15.7 s earlier than the predicted arrival times (Tc: time correction). This time difference is used to allight the synthetic waveforms with he data during the inversion d1-d2) Both phases are detected with high confidence: 3.5 ¡SNR¿ 4.5 (dashed lines), computed with a standard STA-LTA algorithm (window lengths, 10s/100s). This is a M5.0 earthquake that occurred on Feb. 3, 2021 with an epicenter located in the Guinea region (Figure 1) and waveforms recorded by the CTBTO station IM.TOC4 (Figure 2).

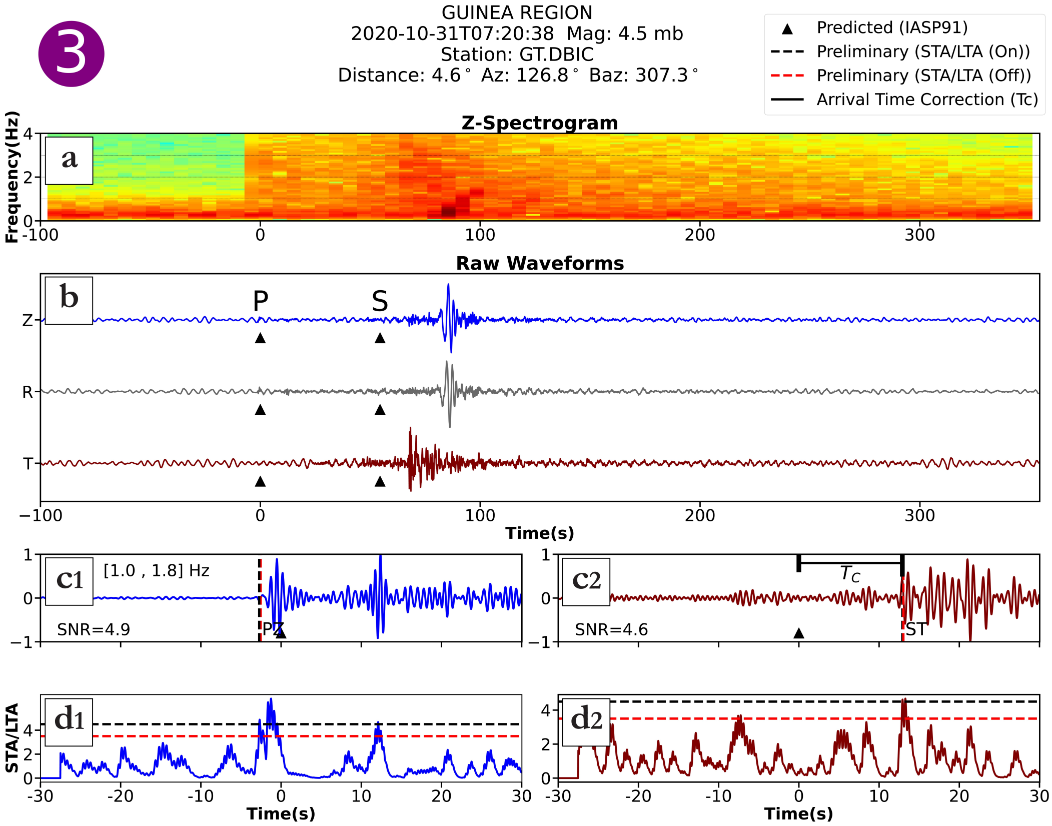

Figure S 4. An example of an automatic phase detection for the Guinea earthquake (M4.5, event 3 in Figure 1 2), medium quality data (compare Figure 2). The phases were detected at frequencies between 1.0 Hz and 1.8 Hz, the highest frequency range used in this study. In this case, the compressional phase was detected 1.2 s before the predicted arrival time. In Figure c1, We noticed that the high-amplitude ground vibration introduced an incorrect pick of the ST phase, because of the lower SNR of a possible S phase arrival near 10 s (-10) before the predicted arrival. This selection is corrected using observations of all the channels of the stations, and the rectilinearity of the signal obtained from polarization analysis.

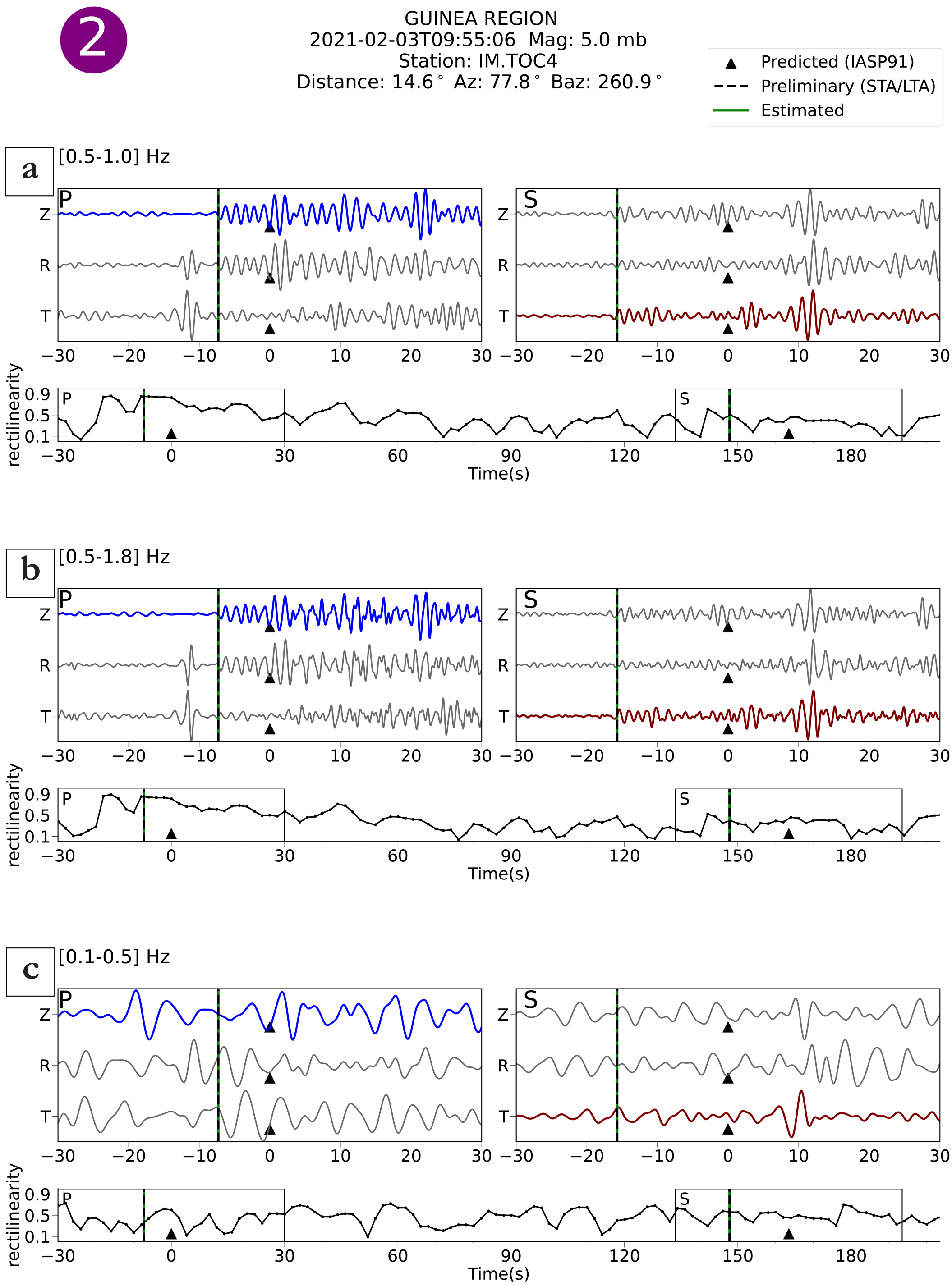

Figure S 5. Seismic waves for the M 5.0 2021-02-03 Guinea earthquake ((2), Figure s 1 and 2), observed at different frequency bandwidths: a) 0.5-1.0 Hz, b) 0.5-1.8 Hz, and c) 0.1-0.5 Hz. The three channels of the station are observed in order to cross-reference the phase picks of PZ and ST with PR, PT, SZ and ST, respectively. The rectilinearity of the phases is used for additional verification of the results of the automatic detection of PZ and ST. In this case, the range 0.5-1.0 Hz is the preferred bandpass interval for the preprocessing of data before the single station inversion for the moment tensor. It is the lowest bandwidth that allows clear identification of the PZ and ST.

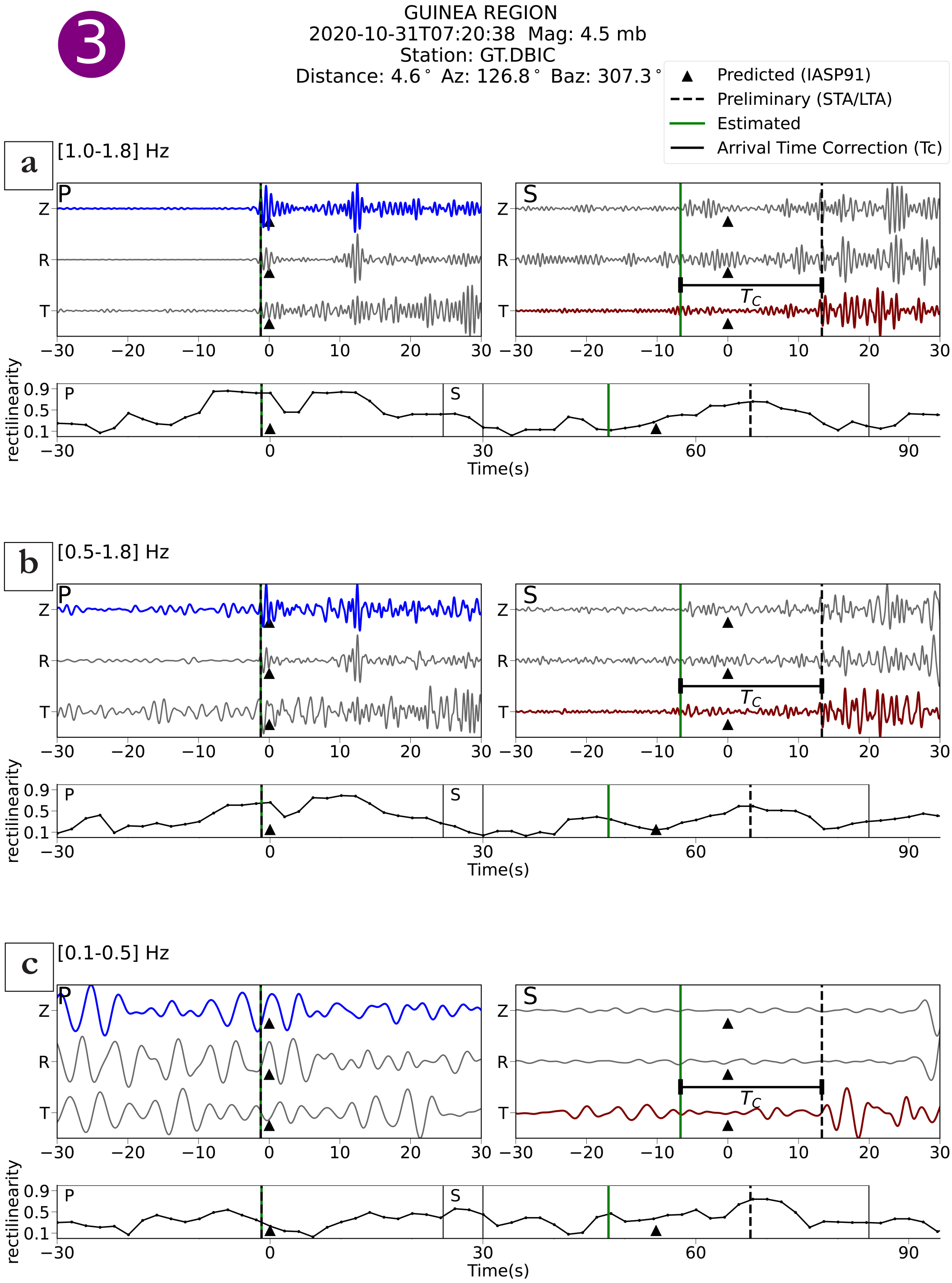

Figure S 6. Seismic waves for the M 4.5 2020-10-30 Guinea Earthquake ((3), Figure s 1 and 2), observed at different frequency bandwidths: a) 1.0-1.8 Hz, b) 0.5-1.8 Hz, and c) 0.1-0.5 Hz. The three channels of the station are observed in order to cross-reference the phase picks of PZ and ST with PR, PT, SZ and ST, respectively. This observation allows a visual estimation of the correct arriva time of the S phase. In this instance, the range 1.0-1.8 Hz is the preferred bandpass interval for the preprocessing of data before the single station inversion for the moment tensor.

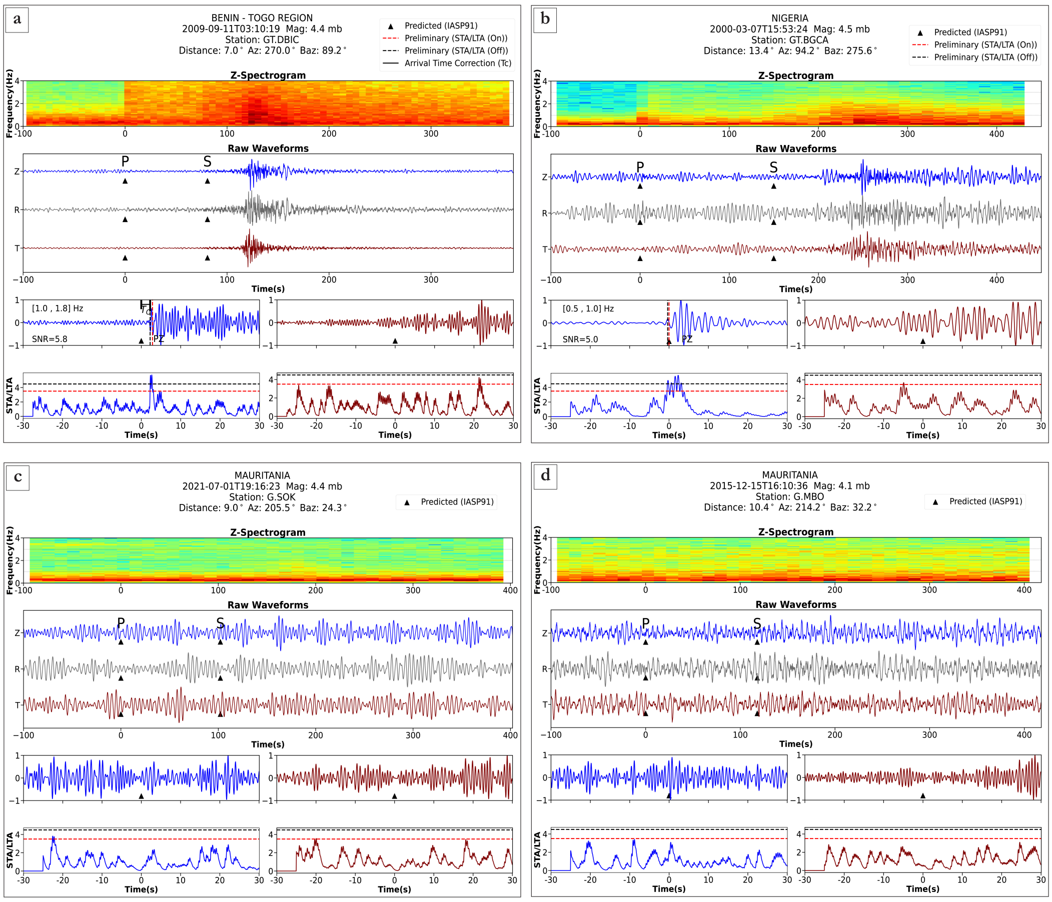

Figure S 7. Examples of low quality (subplots a and b) and undetected (subplots c and d) earthquake signals. a) The STA/LTA pick (vertical black and red dashed lines) of high signal-to-noise ratio (SNR=5.8) PZ , 4.4 seconds after the predicted arrival time (black triangle). The ST phase could not be detected at station GT.DBIC, 7° away from the epicenter of M 4.4 2009-09-11 Benin earthquake ((9), Figure s 1 and 2). The signal-to-ratio of the S phase on the transverse channel is lower than the detection threshold (SNR 4.5). b) Result of the phases detection for the M 4.5 2000-03-07 NIGERIA earthquake, on station GT.BGCA, located 13.4° away from the epicenter. A 5.0-SNR PZ phases is detected, but the ST phase cannot be distinguished from the background noise. c-d) absence of seismic signals from the M 4.4 2021-07-01, and the M 4.1 2015-12-15 Mauritania earthquakes, correspondingly, at stations G.SOK and G.MBO, each located 9.0° and 10.4° away from the respective epicenters.

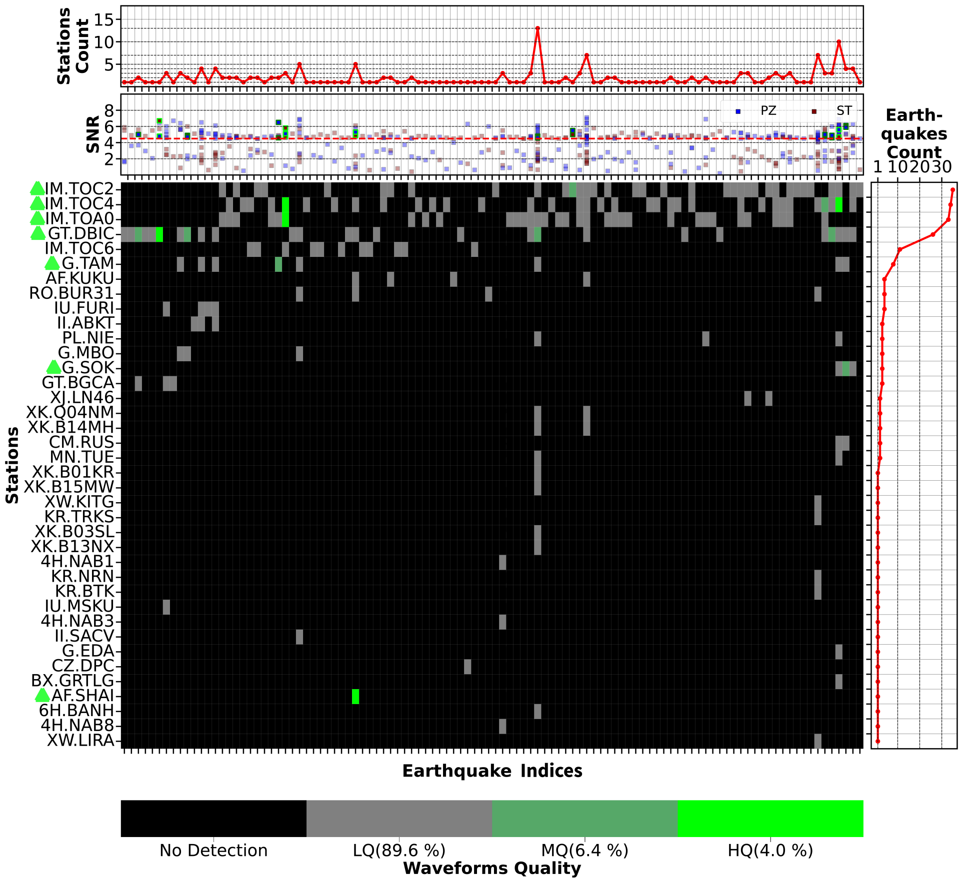

Figure S 8. Heat map of the detection and quality of PZ and ST phases in the inventory of the West African seismic datasets (Figure S1). The plot shows the distribution of results for each earthquake and stations. We only present the stations with at least one seismic phase detection. The M 4.2 2012-08-23 Guinea earthquake ((8), Figure 1) has the highest count of stations with detected earthquake signals (13), based on the criteria in this study. The M 5.0 2021-02-03 Guinea earthquake ((2), Figure 1) is second with 10 stations count.

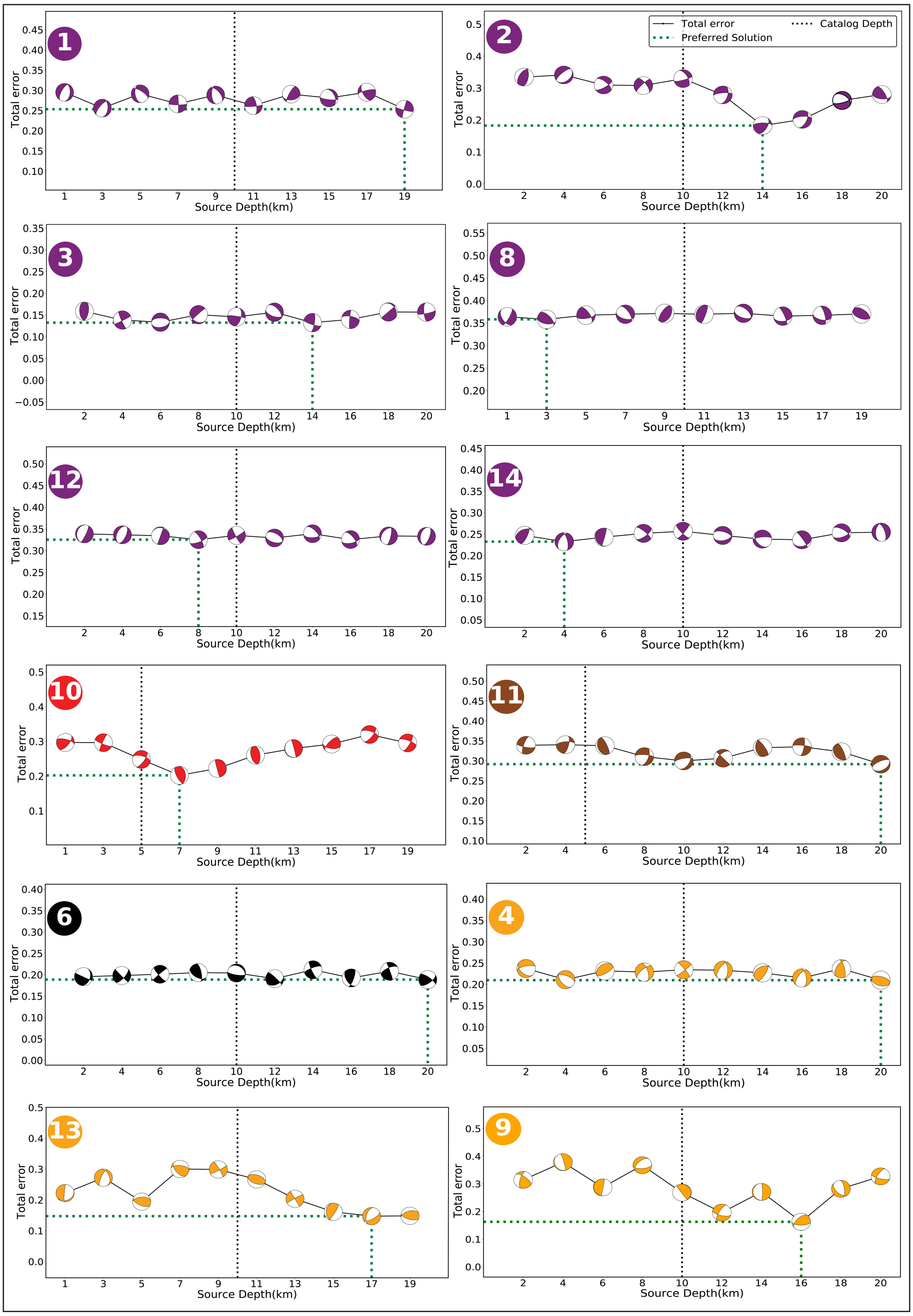

Figure S 9. Source mechanisms of earthquakes (Figure 1 2) resulting from the grid-search inversion of single station data. The solutions are plotted with respect to uncertainty and focal depths. The preferred solution in each case is suggested by the minimum total error (dashed green line). We show the focal depth (black dashed line) reported by public catalogs for comparison.

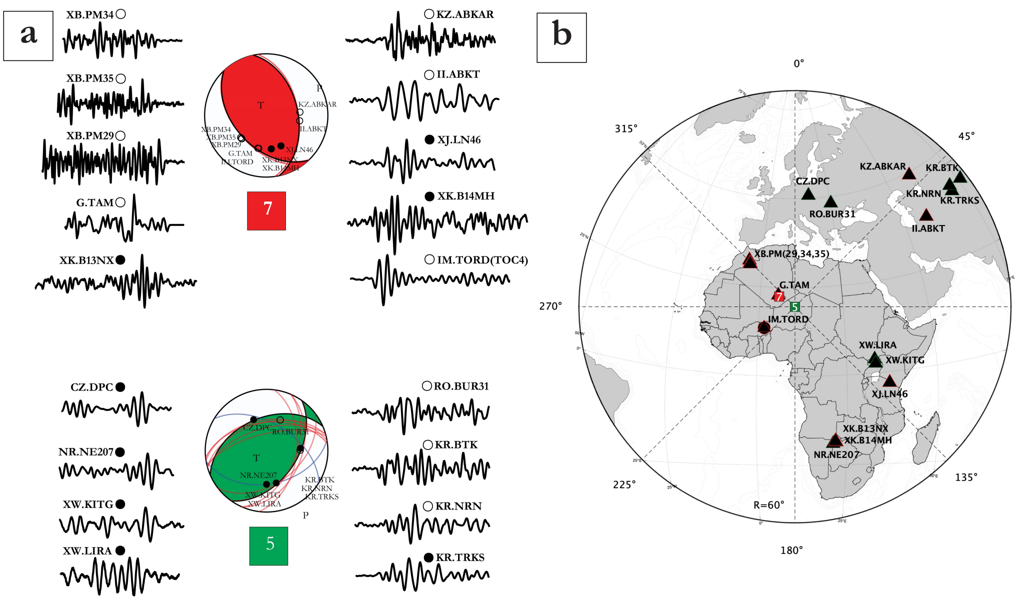

Figure S 10. a) Source mechanism of the M4.5, Valentine 2013 earthquake ((7), Figure 1), in Southern Algeria, and source mechanism of the M4.6, 01/18/2017 earthquake, in Niger ((5), Figure 1). The sources are inverted using the polarity field of the first P-waves (black(+) and white(-) dots) from the listed stations. Both solutions indicate reverse faulting. The robustness of the solutions is confirmed by the Jackknife test, used to assess the stability of the results (red and blue nodal planes, respectively reverse and normal faults).b) Locations of epicenters (indexed squares, Figure 1) and stations (triangle - the edges are colored correspondingly to the earthquakes (5) and (7)) used to compute the source mechanisms.

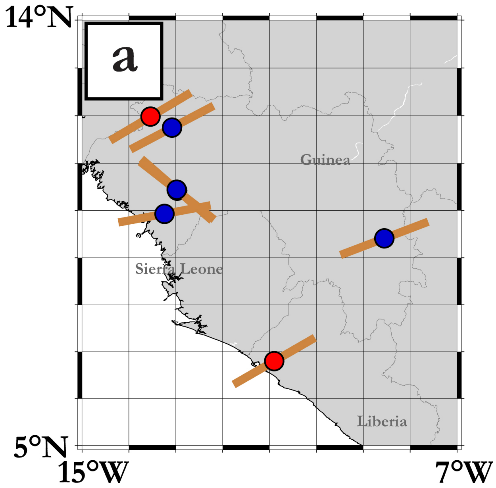

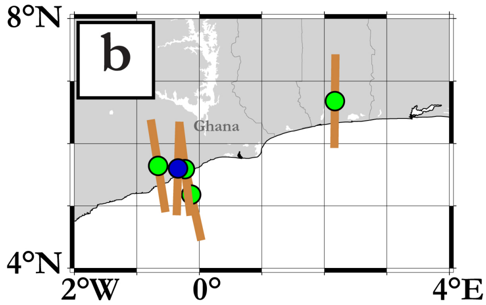

Figure S 11. Stress field from regional inversions for the *Keneman-Man* and the Southern edge of the *WAC*, respectively in a) and b). The stress orientations (golden line) and R' values are averaged and reported in Figure 4f-g. Stress is interpreted as compressional (blue) and strike-slip (green).

Country (Indice)	***Date***	***SHmax***	***R***	***R'***	***Mode***	***TR1***	***TR2***	***TR3***	***PL1***	***PL2***	***PL3***
Kenema-Man Shield (KMS)											
Guinea (1)	2021-05-04	143	0.49	1.51	SS	142	35	53	4	77	12
Guinea (2)	2021-02-03	146	0.43	2.43	TF	156	80	41	20	34	49
Guinea (3)	2020-10-31	53	0.41	1.59	SS	53	143	143	0	61	29
Guinea (8)	2012-08-23	27	0.58	2.58	TF	28	118	116	1	20	70
Guinea (12)	2004-07-02	118	0.64	1.36	SS	117	120	28	31	59	1
Liberia (14)	1995-11-25	21	0.60	0.60	NF	37	7	104	58	29	14
Guinea(☆)	1983-12-22	129(124)	0.36	0.36	NF	21	123	36	61	6	28
Dahomey Shield (DS)											
Ghana (4)	2020-06-24	19	0.55	2.55	TF	20	110	29	18	3	72
Benin (9)	2009-09-11	156	0.46	2.46	TF	161	78	47	13	26	60
Ghana (13)	1997-03-06	37	0.35	0.35	NF	12	46	130	61	24	14
Ghana(☆)	1939-06-22	130(125)	0.50	1.50	SS	130	49	40	1	84	5
Ghana(☆)	1939-06-22	26(16)	0.50	1.51	SS	26	109	116	1	84	6
Gourma Aulacogen (GA)											
Mali (11)	2007-09-15	56	0.37	0.37	NF	1	64	149	64	12	22
Reguibat Shield (RS)											
Mauritania (6)	2013-01-08	177	0.22	1.78	TP	4	106	83	11	44	44
Trans-Saharan Mobile Belt (TSMB)											
Niger (5)	2017-01-18	143	0.68	2.70	TF	142	52	55	1	22	68
Algeria (7)	2013-02-14	62	0.61	2.61	TF	62	153	144	3	17	73
Niger (10)	2008-04-29	70	0.54	2.54	TF	63	147	32	25	13	61

Table S 1. Stress parameters of earthquakes in continental West Africa: the maximum horizontal stress (*SHmax*), the relative stress magnitude (*R'*), the fault types (*Mode*), and the trends and plunges of the principal stresses (*TR1-3*, *PL1-3*). The white stars refer to the historical events in West Africa, see Figure 1. The values of SHmax in the parentheses are from the World Stress Map dataset (?, ?).

Country (Indice)	*Date*	*Lon*	*lat*	*Mag.*	*Depth*	*Strike*	*Dip*	*Rake*
Kenema-Man Shield (KMS)								
Guinea (1)	2021-05-04	-12.98	10.44	4.4	19	104(195)	80(85)	175(10)
Guinea (2)	2021-02-03	-12.97	10.42	5.0	14	269(30)	63(45)	127(40)
Guinea (3)	2020-10-31	-8.55	9.41	4.5	14	10(107)	70(71)	160(21)
Guinea (8)	2012-08-23	-13.08	11.75	4.2	3	99(315)	46(50)	63(115)
Guinea (12)	2004-07-02	-13.24	9.93	3.8	8	329(70)	67(65)	-27(-155)
Liberia (14)	1995-11-25	-10.90	6.80	4.5	4	210(347)	40(58)	-55(-116)
Dahomey Shield (DS)								
Ghana (4)	2020-06-24	-0.34	5.60	4.0	20	285(105)	55(35)	90(90)
Benin (9)	2009-09-11	2.17	6.68	4.4	16	90(225)	55(45)	120(55)
Ghana (13)	1997-03-06	-0.23	5.59	4.4	17	197(60)	38(60)	-126(-65)
Gouma Aulacogen (GA)								
Mali (11)	2007-09-15	-3.74	16.37	3.7	20	60(245)	30(60)	-95(-87)
Reguibat Shield (RS)								
Mauritania (6)	2013-01-08	-12.21	22.71	4.2	20	305(55)	65(54)	140(31)
Trans-Saharan Mobile Belt (TSMB)								
Niger (5)	2017-01-18	10.62	19.62	4.6	10	247(35)	45(49)	113(68)
Algeria (7)	2013-02-14	5.80	22.42	4.5	10	347(136)	47(47)	112(67)
Niger (10)	2008-04-29	3.85	13.85	3.6	17	152(355)	62(30)	79(110)

Table S 2. Fault parameters for earthquakes, sorted by geologic domains, following reported stress information in Table 1. Strikes, dips, and rakes in parentheses refer to the parameters of the auxiliary planes of the focal mechanisms. *Mag.*: Magnitude.

Country	Year	Longitude(°)	Latitude(°)	Depth(km)	Magnitude(M)	Mode	References
Continental West-Africa							
Guinea	1983	-13.54	11.98	10	6.3	NF	(Foster & Jackson, 1998; Suleiman et al., 1993)
Ghana	1939	-0.13	5.18	15	6.5	SS	(Bacon & Quaah, 1981; Suleiman et al., 1993; Yarwood & Doser, 1990)
Ghana	1939	-0.658	5.641	11.8	6.1	SS	
Oceanic West-Africa (Gulf of Guinea)							
Sao T. & Principe	2019	8.21	1.75	29	5.5	TS	Geofon
Gulf of Guinea	1986	-4.89	-0.45	12	5.9	TF	(Suleiman et al., 1993)
North-Atlantic	1971	-20.02	14.9	15	5.4	SS	Harvard CMT
Continental Western-Central Africa							
Cameroon	2005	11.02	4.18	8	4.6	SS	(Ngatchou et al., 2018)
Cameroun	1987	12.95	7.85	15	4.9	TF	Harvard CMT
Congo Brazza	1998	17.4	0.64	15	5.2	TF	(Ayele, 2002)
Congo Brazza	1998	17.04	1.38	10	5	TF	
DRC	2008	25.97	-3.66	10	5.2	SS	Harvard CMT
DRC	1995	19.38	1.13	6	5.5	TF	(Craig et al., 2011)
DRC	2020	24.01	-9.36	42	4.9	NF	USGS
DRC	2020	22.87	-5.39	17	4.7	SS	
DRC	2001	22.71	-6.2	18	4.7	NF	(A. Barth et al., 2007)
DRC	1999	21.6	-8.6		4.6	TF	
DRC	1976	19.336	4.473	23	5.5	TT	(Fairhead & Stuart, 1982)
DRC	1981	22.767	-2.283	8	5.3	SS	Suleiman et al. ,1993
Gabon	2021	10.24	-1.12	10	5	NF	Geofon
Gabon	2021	10.21	-1.06	10	5.3	NF	
Gabon	1974	12.83	-0.282	3	6.1	TF	(Fairhead & Stuart, 1982)
Gabon	1945	15.6	2.5	11	6.1	SS	(Suleiman et al., 1993)

Table S 3. Historical earthquakes in *Continental-West Africa*, *Oceanic West-Africa (Gulf of Guinea)*, and *Continental Western-Central Africa*. Mode indicates faulting styles NF (Normal Fault), SS (Strike-Slip), TT (Transtension, combination of normal and strike-slip fault), and TF (Thrust or reverse faulting).